RESEARCH ARTICLE OPEN ACCESS

Entropy Profiling of Hard Carbon/Na Metal Cells with Stepwise Temperature Changes: Influence of the Sodiation Kinetics on the Cell Voltage Response

Laurin Derr[1] | Steffen Braun[1] | Krishnaveni Palanisamy[2] | Christine Kranz[2] | Rolf Schuster[1]

[1]Institute of Physical Chemistry, Karlsruhe Institute of Technology, Karlsruhe, Germany | [2]Institute of Analytical and Bioanalytical Chemistry, Ulm University, Ulm, Germany

Correspondence: Laurin Derr (laurin.derr@kit.edu) | Rolf Schuster (rolf.schuster@kit.edu)

Received: 24 November 2025 | **Revised:** 21 January 2026 | **Accepted:** 22 January 2026

Keywords: entropy profiling | hard carbon | kinetics | reaction entropy | sodium-ion battery

ABSTRACT

Hard carbon (HC) is commonly used as negative electrode material in sodium-ion batteries. Despite its extensive use, there is still a lack of comprehensive understanding of the sodiation mechanism. To obtain thermodynamic information on the storage processes, the reaction entropy of HC/Na metal cells in $NaPF_6$/diglyme electrolyte solution is determined by measuring the temperature dependence of the equilibrium cell voltage at different states of charge (SoCs), commonly known as entropy profiling. In contrast to former studies, we changed the temperature of the cell stepwise within less than 1 min, which reduces the influence of baseline drift of the cell voltage. The cell reaction entropy varied between −10 and 6 $J\,mol^{-1}K^{-1}$ for all SoCs, which indicates complete solvation/desolvation of the Na^+ ions at the HC composite electrode. In addition, the fast temperature change led to characteristic features of the cell voltage response. These features were explained with a simple model including temperature gradients across the cell and different kinetics of the reactions at the HC and the Na metal electrode. From the cell voltage response, we inferred that the sodiation of HC is significantly slowed down with decreasing SoC.

1 | Introduction

Sodium-ion batteries (SIBs) are considered as future alternative to Lithium-ion batteries (LIBs), due to the abundance and availability of sodium and its drop-in compatibility with existing LIB manufacturing infrastructure [1]. While manufacturers use different chemistries for the positive electrodes (e.g., layered oxides, Prussian blue analogs, or polyanionic compounds) [2], hard carbon (HC) is mainly used as the active material in negative electrodes for commercialization [3]. HC was initially presented by Stevens and Dahn as negative electrode in SIBs [4]. It can be produced from biomass and constitutes nongraphitizable carbon, consisting of graphitic domains, micro- and nanopores, and surface defects [5]. Its properties, such as the morphology, microstructure, and chemical composition, are governed by the precursors as well as the synthesis conditions. The potential profile upon the sodiation of HC can generally be divided into a sloping region, in which the potential steadily decreases from 1.2 V to around 0.1 V (vs. Na^+/Na) with increasing Na content, and a plateau region below 0.1 V, where the potential only slightly varies with the state of charge (SoC) (see Figure 1).

The underlying sodiation mechanism has been studied with various experimental techniques, such as, for example, X-ray scattering techniques [6–14], Raman spectroscopy [7–12, 14–17], infrared spectroscopy [7, 9, 10, 18], solid state NMR [19–23], transmission electron spectroscopy (TEM) [9–11, 24], dilatometry [25, 26] or electrochemical impedance spectroscopy (EIS) [8, 10, 27–31]. Despite these studies, the Na storage mechanism in HC, comprising processes such as adsorption, intercalation, or pore-filling, is still under debate. For instance, it remains unclear, which particular processes are taking place in specific potential

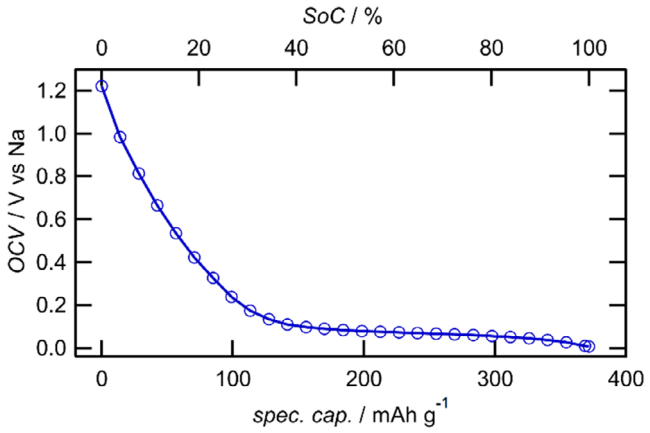

FIGURE 1 | OCV, measured during charging of a HC/Na metal cell. At each data point, the OCV was determined 6000 s after the charging was interrupted. The data points are connected with a line as a guide to the eye.

ranges and to which extent the different sites for Na storage in HC contribute to its capacity [5]. This might result from structural differences among the investigated HCs, a known problem as the precursors used for the HCs determine their microstructure and ultimately their electrochemical behavior.

Thermodynamic information such as the reaction entropy $\Delta_R S$ can contribute to understand and identify the different electrochemical processes. The reaction entropy can, for example, be determined with single electrode microcalorimetry, where the reversibly exchanged heat during an electrochemical reaction is directly measured at the working electrode (WE). With this approach, we investigated the sodiation/desodiation of HC in sodium perchlorate ($NaClO_4$)/propylene carbonate (PC) as well as sodium hexafluorophosphate ($NaPF_6$)/diglyme electrolyte solution in a previous study [32]. We found positive reaction entropies for the cathodic process at the single electrode (up to 85 and 250 $J\,mol^{-1}K^{-1}$ for PC and diglyme, respectively) caused by the concomitant desolvation of the Na^+ ions during sodiation of HC. Due to experimental constraints, the timescale of this method is restricted to below ca. 1 s, therefore, slower processes are not or not fully captured.

The timescale of the entropy measurement can be extended by using so-called entropy profiling, where the temperature dependence of the equilibrium cell voltage E_0 is measured to determine the reaction entropy of the complete cell [33, 34].

$$\Delta_R S_{cell} = -\left(\frac{\partial \Delta_R G}{\partial T}\right)_{p,n_i} = zF\left(\frac{\partial E_0}{\partial T}\right)_{p,n_i} \approx zF\frac{\Delta E_0}{\Delta T} \qquad (1)$$

Herein $\Delta_R G$ is the free reaction enthalpy, T is the temperature, z is the number of transferred electrons, and F is the Faraday constant. In principle this method is only limited by the stability of the system, and since the system is probed in an equilibrium state, all processes, independent of their timescale, should be completed. In practice, drifting open circuit voltage (OCV), due to, for example, slow diffusion processes in the HC composite electrode, makes it difficult to reach full equilibration, and only metatable states are attained and can be probed at reasonable timescales. It should be noted here that the resulting $\Delta_R S_{cell}$ is the sum of the reaction entropies of the processes taking place at the WE and the reference electrode (RE), which gives the net entropy change of the complete cell. In the following, we use the term complete cell for an electrochemical cell consisting of the HC composite, the Na metal electrode, and the electrolyte solution, and the term single electrode for one electrode immersed into the electrolyte solution.

Already in the early 80ties, Dahn et al. applied entropy profiling to investigate Li metal/$LiTiS_2$ cells [33]. More recently, it has been used by several groups to determine $\Delta_R S_{cell}$ of HC/Na metal cells with different electrolyte solutions at varying SoCs [35–38]. While the entropy can be determined quite precisely in plateau regions of the charging curve, uncertainties about the results remain at SoCs, where a constant OCV is difficult to reach within the measurement time. During the sodiation of HC, this is the case for the sloping region at low SoC, where the OCV drifts significantly after charging or discharging, which might be attributed to slow diffusion processes [29] or self-discharge processes, such as, for example, SEI dissolution [39, 40].

Typical measurement times in entropy profiling amount to several 10 min, mostly determined by the heating or cooling rate of the thermostat or measurement chamber during the temperature variation. As a consequence of these slow temperature changes, the equilibrium cell voltage variations due to the changes in temperature become superimposed by simple drift of the OCV. This problem might be solved by background fitting, that is, reconstruction of the cell voltage curve at the initial temperature, as shown by Osswald et al. for commercial LIBs [41]. However, this involves careful evaluation of the SoC-dependent drift for each investigated system.

In this study, we use a different approach and changed the temperature of a HC/Na metal coin cell with 1 M $NaPF_6$ in diglyme electrolyte solution within less than 1 min by switching between two thermostats to reduce the influence of slow OCV drift. This rather abrupt temperature variations allow us to evaluate how slow diffusion processes of, for example, Na in the HC composite electrode, or sluggish charge–transfer reactions may influence the measured variation of the cell voltage with temperature. The sodiation of HC suits well for this study, since the charging curve consists of a sloping and a plateau region with different sodiation mechanisms with presumably different relaxation times. With a simple model, we show how the equilibration of the respective single electrode potentials upon switching of the temperature is reflected in the measured cell voltage. We further present the influence of the OCV drift on the determined reaction entropy and a comparison with recent publications on entropy profiling of the sodiation of HC.

2 | Results and Discussion

2.1 | Cell Voltage Transients upon Temperature Steps at Different SoCs

In Figure 1, the OCV of a HC/Na metal cell with $NaPF_6$/diglyme electrolyte solution during an intermittent charging cycle is shown as a function of the SoC. The charging at 0.05 C rate was periodically interrupted, and the OCV was measured 6000 s after each interruption. The sloping and plateau regions are apparent. At each SoC, the temperature of the cell was switched from 25.0°C to 20.7°C after the 6000 s resting phase, and then it was switched back to the initial temperature after

an additional 1000 s (compare Figure 2e). Switching between two heat reservoirs (see Experimental Section) enables temperature changes of the electrodes within less than 1 min, as discussed below in more detail (see also Figure 2e). The resulting transients of the cell voltage due to the temperature steps are exemplarily shown for four different SoCs in Figure 2a–d. For the fully sodiated HC (Figure 2a, SoC 99%, blue line) a new voltage plateau can be clearly identified about 60 s after the temperature change, which lies about 0.46 mV more positive than the initial cell voltage. Directly after the temperature change, a sharp negative voltage spike is visible, which is leveling off within a few 10 s (see inset in Figure 2a). Applying twice the temperature difference led to a doubling of the cell voltage responses, that is, of the magnitude of the sharp spike as well as of the shift of the cell voltage plateau (see Figure S2). As it will be discussed in detail below, we attribute the sharp voltage spike to temperature gradients inside the cell during the switching of the temperature, which are expected to be proportional to the temperature variations. We attribute the shift of the voltage plateau at $t > 60$ s to the reaction entropy of the cell, which is related to the temperature coefficient of the equilibrium cell voltage by Equation (1). From the cell voltage shift in Figure 2a, we calculated a reaction entropy of the complete HC/Na metal cell of $-10.3\ \mathrm{J\ mol^{-1}K^{-1}}$. When reversing the temperature step at $t \geq 1000$ s the voltage variation reverses correspondingly. The cell voltage transient in Figure 2a is typical for all SoCs in the plateau region ($30\% < \mathrm{SoC} < 100\%$). At these SoCs, the cell voltage reached a clearly identifiable steady value, ca. 60 s after the temperature was switched. With these well-defined voltage shifts the complete cell reaction entropy could be determined according to Equation (1). We found values between −10 and $+6\ \mathrm{J\ mol^{-1}K^{-1}}$ as discussed below in detail.

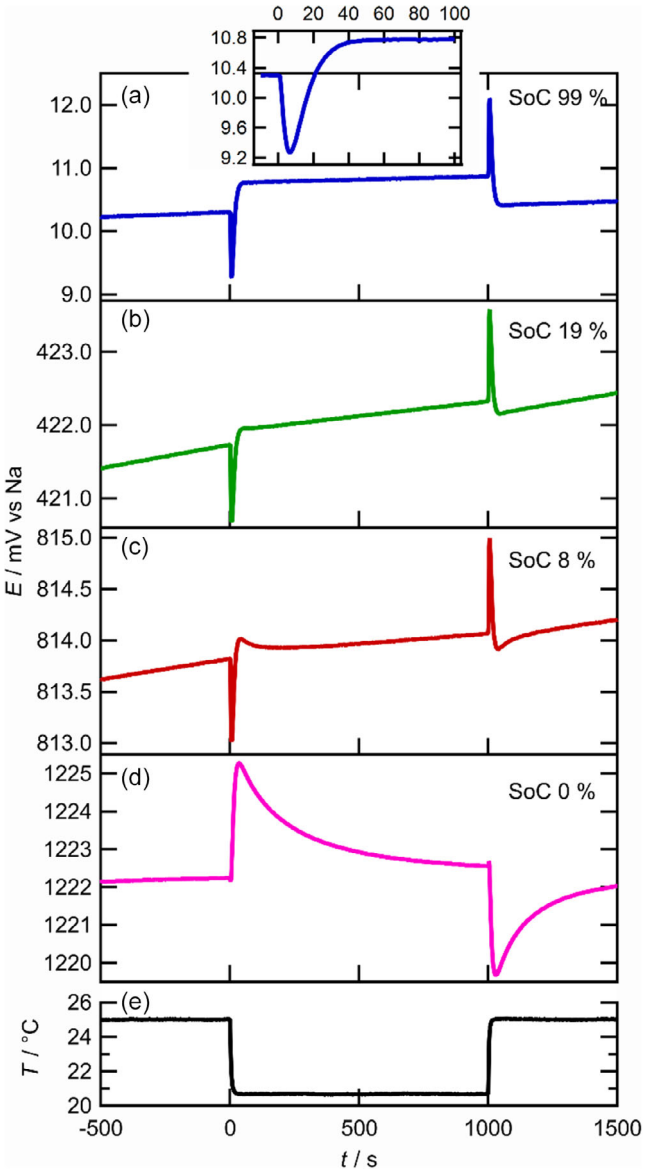

FIGURE 2 | (a–d) Cell voltage transients at open circuit conditions caused by temperature steps. The panels (a–d) correspond to different SoCs during the charging cycle. The inset in (a) shows the cell voltage minimum in detail. (e) Temperature of the aluminum cell holder.

At lower SoC in the sloping region (Figure 2b, SoC 19%, green line), the overall shape of the cell voltage transients followed the same behavior, that is, a short voltage spike followed by a plateau region. However, the OCV drift increased to ca. $0.6\ \mu\mathrm{V\ s^{-1}}$, which hampers a direct evaluation of the temperature-induced voltage shift. At even lower SoC (Figure 2c, SoC 8%, red line), in addition to the pronounced OCV drift, the new cell voltage plateau is reached after passing a small (0.19 mV) maximum at $t = 40$ s, which decays within 300 s. For fully desodiated HC (Figure 2d, SoC 0%, pink line), the cell voltage response to the temperature step is dominated by a large maximum (3.03 mV) extending to the end of the temperature step at $t = 1000$ s and a new voltage plateau was not reached within that time span.

We can conclude that the shape of the measured voltage transients following stepwise temperature variation is strongly dependent on the SoC. Deviations from ideal stepwise behavior can be categorized into (i) sharp voltage spikes occurring on a timescale $t < 10$ s after the beginning of the temperature step, (ii) baseline drift of the OCV, and (iii) the evolution of a wide but small maximum at $t \approx 40$ s, which (iv) at SoCs below 8% turns into an extended maximum dominating the cell voltage response. All characteristics change sign upon reversal of the temperature step. In the following, we will try to rationalize these deteriorations by introducing a simple model, explaining the cell voltage response upon temperature steps.

2.2 | Single Electrode Potential Simulation

The variation of the cell voltage E of the HC/Na metal cell at open circuit conditions upon application of a temperature step, starting from T_0, is given by the difference between the variations of both single electrode potentials, $\Delta\phi_{\mathrm{HC}}$ and $\Delta\phi_{\mathrm{Na}}$, which both depend on the actual temperatures of the single electrodes, T_{HC} and T_{Na}

$$\Delta E = \Delta\phi_{\mathrm{HC}}(T_{\mathrm{HC}} - T_0) - \Delta\phi_{\mathrm{Na}}(T_{\mathrm{Na}} - T_0) \qquad (2)$$

Note that the brackets in Equation (2) indicate the functional dependency of the potential variations on the temperature differences. When the equilibration of the single electrode potentials is assumed to be infinitely fast, they correspond to the single electrodes' equilibrium potentials $\phi_{0,\mathrm{HC}}$ and $\phi_{0,\mathrm{Na}}$. Their temperature dependence is given in analogy to Equation (1). This results in an

actual variation of the cell voltage with the electrode temperatures, starting from the equilibrium cell voltage where both electrodes are at temperature T_0. For simplicity we assume that the entropies of the single electrode reactions remain constant upon the temperature variations of 4.3 K applied herein.

$$\Delta E = \frac{\partial \phi_{0,\mathrm{HC}}}{\partial T} \cdot (T_{\mathrm{HC}} - T_0) - \frac{\partial \phi_{0,\mathrm{Na}}}{\partial T} \cdot (T_{\mathrm{Na}} - T_0)$$
$$\approx \frac{1}{zF} \Delta_R S_{\mathrm{HC}} \cdot (T_{\mathrm{HC}} - T_0) - \frac{1}{zF} \Delta_R S_{\mathrm{Na}} \cdot (T_{\mathrm{Na}} - T_0) \quad (3)$$

Note at this point that for a correct description of the cell voltage upon temperature gradients across the cell, ion and electron transport across the borders of the single electrodes have to be included, which necessitates description in terms of irreversible thermodynamics. However, since the involved entropies of transport are below 10% of the single electrode reaction entropy in our case (see discussion in Ref. [42]) and since we are dealing here with a rather qualitative discussion, we ignore these corrections in the following. For a more detailed treatment see, for example, Agar [43].

In case of equal temperatures at both electrodes ($T_{\mathrm{HC}} = T_{\mathrm{Na}}$) and since $\Delta_R S_{\mathrm{HC}} - \Delta_R S_{\mathrm{Na}} = \Delta_R S_{\mathrm{cell}}$, Equation (3) becomes equivalent to Equation (1). However, for different electrode temperatures, not only differences in the single electrode reaction entropies, but also differences in the electrode temperatures will be reflected in the measured cell voltage. Indeed, in entropy profiling experiments, such temperature differences of the electrodes are naturally expected during changing the temperature, due to asymmetric heat transfer within a typical cell. For example, in our cells, the HC composite electrode is directly pressed against the cell housing, while the Na electrode is contacted via a spring with low thermal conductivity (see Figure S3). We thus expect that in our experiments the HC composite electrode will follow the temperature step much faster than the Na electrode. This is corroborated by a simulation of the thermal responses of the electrodes assuming that the heat flux towards the Na electrode occurs purely through the electrolyte-soaked separator and the HC composite electrode (details are given in the supporting information). Figure 3a shows the simulated temperature evolution of both electrodes. It can be clearly seen that we expect significant differences of the electrode temperatures up to about 60 s. A pronounced minimum of the temperature difference of about −2.5 K evolved at $t = 7$ s.

Assuming that the adjustment of the single electrode potentials is fast, we employed Equation (3) to simulate the electrode potentials and the variation of the cell voltage with time directly from the electrodes' temperature variations reported in Figure 3a. We used a reaction entropy for Na metal deposition of $\Delta_R S_{\mathrm{Na}} = 234\ \mathrm{J\ mol^{-1}K^{-1}}$ as determined in a previous microcalorimetry study [42]. Since for a SoC of 99% we found $\Delta_R S_{\mathrm{cell}} \approx -10\ \mathrm{J\ mol^{-1}K^{-1}}$ above (see Figure 2a), we employed an entropy of $\Delta_R S_{\mathrm{HC}} = 224\ \mathrm{J\ mol^{-1}K^{-1}}$ for the sodiation of the fully sodiated HC composite electrode. As discussed in References [32, 42], the reaction entropies of the HC and the Na metal electrode reaction are dominated by the desolvation entropy of the Na^+ ions. When considering the complete cell, during the charging process desolvation of Na^+ takes place at the HC composite electrode, while solvation of Na^+ will happen at the Na metal electrode. Thus, these entropy contributions mostly compensate for each other, which leads to the rather small values of the complete cell reaction entropy $\Delta_R S_{\mathrm{cell}}$. The results of the potential simulation are shown in Figure 3b. The single electrode potentials directly follow the respective temperature profiles and end up with a difference of about 0.4 mV for $t > 80$ s, which can be directly attributed to the difference of the reaction entropies at the two electrodes, that is, $\Delta_R S_{\mathrm{cell}}$. However, at $t = 7$ s, the cell voltage exhibits a pronounced minimum, lower than −5 mV, which can be directly attributed to the differing time evolution of the two electrode temperatures. The simulated behavior is very similar to the experimentally observed minima in Figure 2a,b for the fully and intermediately sodiated HC. Note that due to the high reaction entropies of the single electrodes, the single electrode potentials are strongly varying by more than 10 mV. Nevertheless, after equilibration, that is, when temperature gradients have vanished, the change in the cell voltage amounts only to a few hundred of microvolts. In conclusion, in our experiment we attribute the sharp negative cell voltage spike at $t < 10$ s to the evolution of temperature gradients across the coin cell and the resulting strong variations of the single electrode potentials. For $t > 60$ s

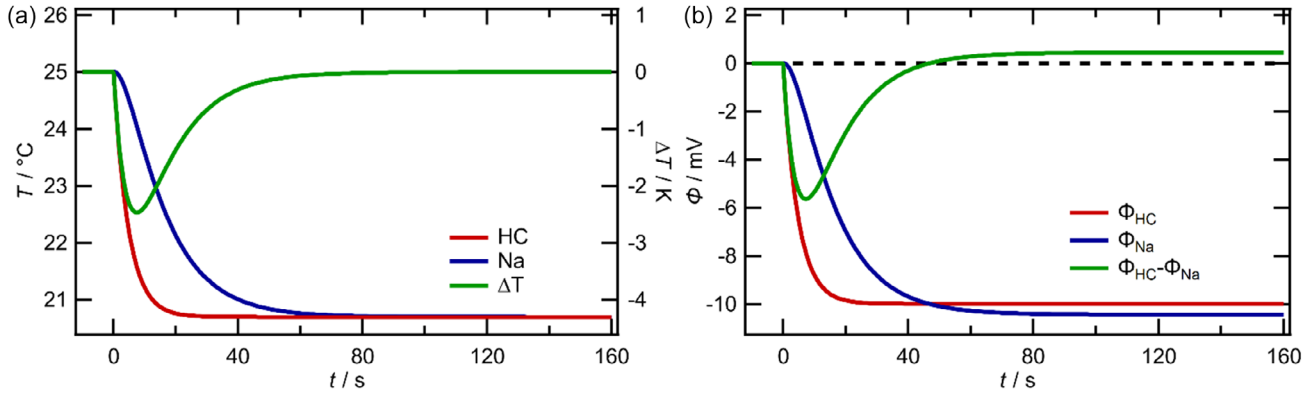

FIGURE 3 | (a) Simulated temperature transients of the HC composite electrode (red) and the Na metal electrode (blue) and their temperature difference (green) caused by an exponential decay of the temperature at the backside of the HC composite electrode by 4.3 K. (b) Single electrode potentials (red and blue) and cell voltage (green) resulting from the simulated electrode temperatures in (a), calculated from Equation (3). This assumes that the equilibration of the single electrode potentials is fast. For the single electrode reaction entropies $\Delta_R S_{\mathrm{Na}} = 234\ \mathrm{J\ mol^{-1}K^{-1}}$ and $\Delta_R S_{\mathrm{HC}} = 224\ \mathrm{J\ mol^{-1}K^{-1}}$ were used.

these temperature gradients vanish and both electrodes reach the same temperature.

However, upon temperature steps at a SoC of 8% the negative voltage spike was followed by a maximum, which at a SoC of 0% even dominated the cell voltage response (c.f. Figure 2c,d). Such a maximum could not be explained with the simulations described so far, in which we assumed that the single electrode potentials can instantaneously follow the temperature variation according to Equation (3). It should be noted at this point that the sodiation or desodiation of HC has been reported to be kinetically hindered at such low SoCs, which reflects itself in a high charge–transfer resistance in EIS (e.g., at 0% SoC values of 5 kΩ cm^2 [8] and 330 Ω cm^2 [31] were reported in the literature). We therefore suppose that kinetic limitations of the processes at the HC composite electrode may cause the cell voltage maximum. In order to examine this hypothesis, we included the kinetics of the electrode processes in our simulation. As shown above, changing the temperature of a single electrode leads to a strong variation of its potential (c.f. Figure 3b). Thus, the single electrodes' double layers have to be rather strongly polarized upon the temperature changes in order to readjust thermodynamic equilibrium. In other words, a small amount of Na^+ has to be either inserted or extracted from the electrode in order to change the polarization of the double layer.

In order to account for double layer polarization in our simulation, we assumed a simple Butler-Volmer type kinetics for the electrode processes (exemplarily shown here for the sodiation/desodiation of the HC composite electrode). The overpotential to drive the reaction is given by the difference between the temperature-dependent single electrode equilibrium potential $\phi_{0,\mathrm{HC}}(T_{\mathrm{HC}})$ as employed in Equation (3) and the actual electrode potential ϕ_{HC}. The current density referring to the active electrode area is given by [44]

$$j = zFc_0k_0\left(\exp\left(\frac{\alpha F(\phi_{\mathrm{HC}}-\phi_{0,\mathrm{HC}}(T_{\mathrm{HC}}))}{RT}\right) - \exp\left(-\frac{(1-\alpha)F(\phi_{\mathrm{HC}}-\phi_{0,\mathrm{HC}}(T_{\mathrm{HC}}))}{RT}\right)\right) \quad (4)$$

with the standard concentration $c_0 = 1\ \mathrm{mol\ l^{-1}}$, the transfer coefficient α, which was set to 0.5, the molar gas constant R and the standard rate constant $k_0 = A\exp\left(-\frac{\Delta H^{\ddagger}}{RT}\right)$. Herein, $\Delta H^{\ddagger}$ is the activation energy and A is the preexponential factor, which is assumed to be temperature-independent. Using Equations (3) and (4), we simulated the single electrode potentials of the HC composite and the Na metal electrode for the temperature transients shown in Figure 3a. We neglected any concentration changes, since we did not expect large conversions for double layer polarization. As capacitance of the double layer, we estimated about 100 μF cm^{-2} taking the active electrode area into account.

For fully sodiated HC and Na metal, values for $\Delta H^{\ddagger}$ and A, were available. With temperature-dependent EIS studies Niu et al. determined them for a Na metal electrode (59.0 kJ mol^{-1}, 79,000 m s^{-1}) [45], and Lv et al. for a fully sodiated HC composite electrode (64.0 kJ mol^{-1}, 711 m s^{-1}) [27]. With these kinetic parameters the polarization of the electrodes occurs more or less instantaneously on the timescale of the temperature variation, and the simulated single electrode potential and the cell voltage transients shown in Figure 4a (referred to as high SoC) are identical to the simulations disregarding the polarization reaction (see Figure 3b). The simulated transient of the cell voltage very much resembles those experimentally observed for high SoCs, that is, between about 30% and 100% (see, e.g., Figure 2a). Note here, that the depth of the sharp cell voltage minimum is about five times larger in the simulation than in the experiment (cf. Figure 2a). This could be attributed to an unreasonably slow heat transfer to the Na electrode in the simulation, since, for example, heat transfer via the spring from the backside of the Na metal electrode is neglected. Alternatively, the activation energy for the sodiation of HC at high SoC may have been underestimated. A higher activation energy would lead to a slower equilibration of the potential of the HC composite electrode and thus to a less pronounced voltage minimum.

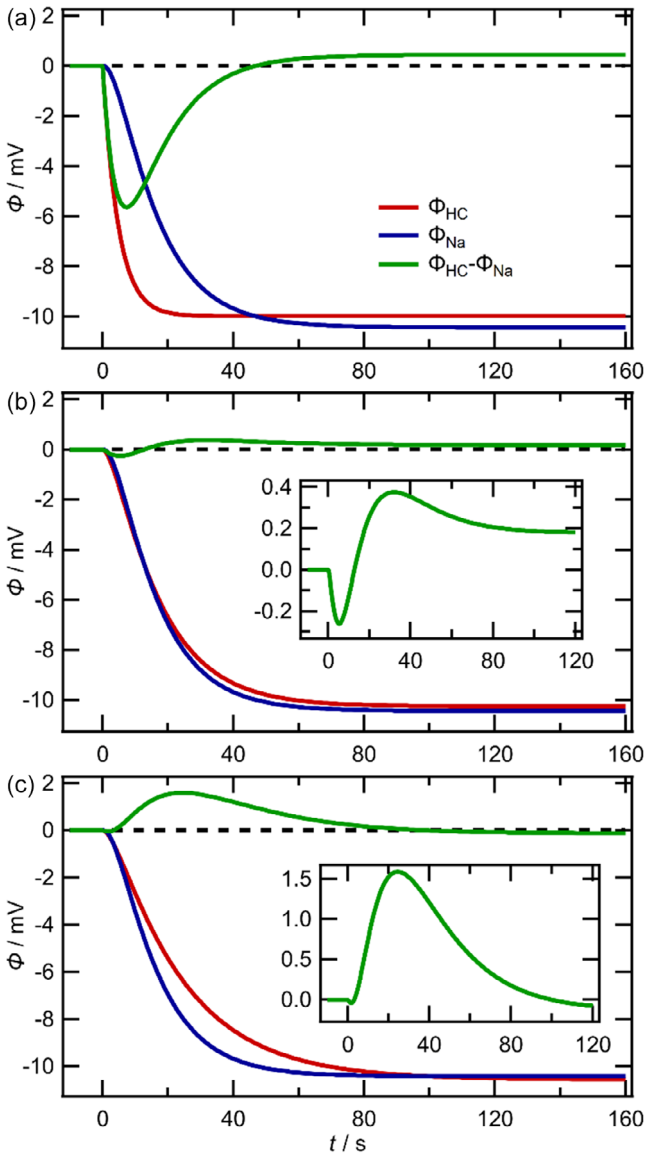

FIGURE 4 | Simulated single electrode potentials of the Na (blue line) and the HC (red line) electrode together with the resulting cell voltage (green line) for different SoCs. The employed reaction entropies and activation energies for the HC composite electrode reaction were: (a) high SoC, 224 J mol^{-1}K^{-1}, 64.0 kJ mol^{-1}; (b) medium SoC, 230 J mol^{-1}K^{-1}, 76.5 kJ mol^{-1}; and (c) low SoC, 237 J mol^{-1}K^{-1}, 77.5 kJ mol^{-1}.

For lower SoCs, where we expect contributions from slow sodiation kinetics, no kinetic data were available in the literature for the same electrolyte solution. We therefore adjusted the activation barrier in our simulation to fit the experimentally observed behavior for a SoC of 8% (referred to as medium SoC in the simulation) and a SoC of 0% (referred to as low SoC). We achieved qualitative agreement between the simulated and the experimentally observed cell voltage transients with $\Delta H^{\ddagger} = 76.5\ \mathrm{kJ\ mol^{-1}}$ at medium SoC and $77.5\ \mathrm{kJ\ mol^{-1}}$ at low SoC. In particular, we aimed to replicate the minima and maxima of the cell voltage transients, as it will be discussed in detail below. The increased activation barrier at low SoCs is in accordance with temperature-dependent EIS measurements of Aniskevich et al. [8], who found that the activation energy of the charge transfer process at HC composite electrodes in a PC-based electrolyte solution increases from high to low SoC.

The simulated single electrode potential and cell voltage transients for medium and low SoC are shown in Figure 4b,c. In both cases, the decrease of the simulated electrode potential of the HC composite electrode is considerably delayed with respect to its temperature transient, which is a direct consequence of the hindered sodiation rate at lower SoC and consequent slow double layer charging. The slowdown of the potential variation of the HC composite electrode has considerable consequences for the change of the cell voltage. At medium SoC (Figure 4b) the sharp negative voltage spike, which was attributed to the temperature gradient across the cell, is significantly reduced in its amplitude. A maximum of the cell voltage evolved at around 30 s and leveled off within about 100 s. This is similar to the experimental results shown in Figure 2c for 8% SoC. At low SoC (Figure 4c) with even slower polarization of the HC composite electrode, the sharp negative voltage spike of the transient of the cell voltage almost vanished and the maximum had a larger amplitude and extended to more than 100 s, comparable to the experimental results obtained at 0% SoC (Figure 2d).

In conclusion, due to the high single electrode reaction entropies, the single electrode potentials vary considerably upon the temperature step, which firstly explains the sharp cell voltage minimum at $t < 10$ s, reflecting temperature gradients across the coin cell. Secondly, the pronounced maximum of the cell voltage at around 30 s, which was observed for lower SoCs of the HC, could be ascribed to sluggish kinetics of the sodiation processes of HC, which is in agreement with EIS studies [8, 31].

2.3 | OCV Drift After Charging/Discharging

A remaining obstacle for the quantitative determination of the cell reaction entropy is the OCV drift at SoCs in the sloping region (0%–30%), which is significant even 6000 s after the charging/discharging was interrupted. This problem is exemplarily discussed using the cell voltage transients shown in Figure 5 at an SoC of 19%. One transient was measured during the charging cycle (Figure 5a) and the other one during the discharging cycle (Figure 5b). Both transients exhibit a rather stepwise change of the cell voltage upon application of the temperature step, after $t > 60$ s, when temperature gradients have vanished. The dashed lines indicate the drift of the OCV before (red, linear fit from $t = -500$ s to $t = 0$ s) and after the temperature step (blue, linear fit from $t = 300$ s to $t = 1000$ s). In the charging cycle the OCV drift

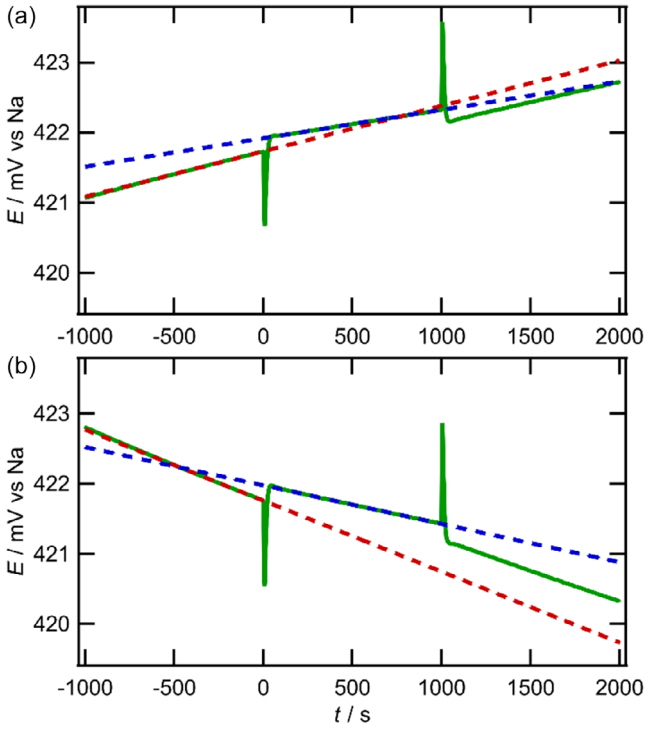

FIGURE 5 | Cell voltage transients at open circuit conditions caused by temperature steps during the (a) charging and the (b) discharging cycle at an SoC of 19%. The red dashed lines indicate the drift of the cell voltage at the initial temperature (25.0°C, linear fit from $t = -500$ s to $t = 0$ s). The blue dashed lines give the drift at the lower temperature (20.7°C, linear fit from $t = 300$ s to $t = 1000$ s).

is positive, whereas during the discharging cycle it is negative. In both cases, the OCV drift is slower, when the cell is at the lower temperature ($0.4\ \mu\mathrm{V\ s^{-1}}$ vs. $0.6\ \mu\mathrm{V\ s^{-1}}$ in Figure 5a and $-0.5\ \mu\mathrm{V\ s^{-1}}$ vs. $-1.0\ \mu\mathrm{V\ s^{-1}}$ in Figure 5b). This is expected, since we ascribe the relaxation of the OCV to thermally activated processes, such as equilibration of the Na concentration in the HC composite electrode by diffusion, or SEI dissolution processes. Note here that after switching back to the initial temperature for $t > 1000$ s, the slope of the drift adopts again its initial value, that is, the red dashed lines in Figure 5a,b are approximately parallel to the courses of the cell voltages for $t > 1000$ s. It is evident from Figure 5 that the temperature-dependent base line drift of the OCV impedes the determination of the cell voltage variation with temperature. Therefore, special care of the OCV drift should be taken during data evaluation when entropy profiling results of the charging cycle differ from those of the discharging cycle. In this work, for the determination of the voltage shift due to the temperature step, we extrapolated the cell voltage plateau at the lower temperature to $t = 0$ s to eliminate the influence of the base line drift. Note that in conventional entropy profiling experiments, the variation of the cell temperature takes of the order of 10 min during which baseline drift cannot be determined [41].

2.4 | Cell Reaction Entropy of the HC/Na Metal Cell

Based on the discussion above, we now extract entropy values from the cell voltage transients measured at the different SoCs

for our HC/Na metal cell as exemplarily shown in Figure 2. For SoCs ≥ 8%, the plateau region with the new equilibrium cell voltage can be clearly identified. In these cases, we applied a linear fit between $t = 300$ s and $t = 1000$ s, that is, starting after the cell voltage deteriorations due to temperature gradients and sluggish sodiation kinetics as discussed above. This fit was then extrapolated to $t = 0$ s and the difference to the measured cell voltage at the higher temperature at $t = 0$ s was adopted as ΔE_0 (see, e.g., Figure S4), from which $\Delta_R S_{cell}$ was calculated according to Equation (1). For SoCs below 8%, such a linear regime of the cell voltage transients was not reached within the measurement time and ΔE_0 couldn't be derived (see, e.g. Figure 2d). Instead, it was estimated from experiments with prolonged waiting time (3500 s) after switching the temperature of the cell to 20.7°C, resulting in $\Delta_R S_{cell}$ values between −7 to +4 J mol^{-1}K^{-1} for 0% SoC and −5 to +2 J mol^{-1}K^{-1} for 4% SoC.

In Figure 6, the resulting $\Delta_R S_{cell}$ values for SoCs ≥ 8% are shown together with the respective OCV for a complete charging/discharging cycle. With increasing SoC, the entropy reaches a minimum (−4.3 J mol^{-1}K^{-1}), followed by a maximum (+6.2 J mol^{-1}K^{-1}) in the middle of the potential plateau and finally decreases to its lowest value of about −10.4 J mol^{-1}K^{-1} when the HC composite electrode is fully sodiated. Similar entropy variation could be identified in the discharging cycle, but the minimum at low SoC is slightly below this minimum in the charging cycle (−5.3 compared to −4.3 J mol^{-1}K^{-1}). Plotting $\Delta_R S_{cell}$ versus the OCV (see Figure S5) shows that at OCVs between 0.1 and 0.5 V the entropy values determined in the charging cycle are slightly above those of the discharging cycle. This might be a remaining artifact due to the pronounced OCV drift in this region as explained above. The repeatability of the experiment was evaluated by measuring the same coin cell with an increased temperature step height (9.2 K), and the reproducibility by measuring a second cell produced from the same batch of HC composite material. Highly consistent results with a maximum deviation below 1 J mol^{-1}K^{-1} were found (see Figure S6).

Since the obtained reaction entropy of the complete cell is rather small, the single electrode reaction entropy of the HC composite electrode has to be of similar magnitude as the one of the Na metal electrode. For SoCs above 20%, this is in accordance with our previous microcalorimetry study, in which we determined the sodiation entropy of HC by measuring the reversibly exchanged heat directly at the electrode [32]. For SoCs below 20%, up to 130 J mol^{-1} K^{-1} lower values were found with microcalorimetry. These low values were explained by an incomplete desolvation within the short timeframe (<0.4 s) captured by the microcalorimetric method. Since the herein measured $\Delta_R S_{cell}$ is close to zero also at SoCs below 20%, we can assume that the solvation/desolvation is completed within the applied measurement time of about 300 s.

Several studies proposed a solvent cointercalation mechanism of Na^+ in HC in ether-based electrolyte solutions based on TEM, X-ray diffraction, and X-ray photoelectron spectroscopy results [7, 10, 27]. Such a solvent cointercalation would lead to significant differences between the reaction entropies of both single electrodes, because the Na^+ ions would be only partially desolvated at the HC composite electrode, whereas full solvation would naturally take place at the Na metal electrode upon Na dissolution. Since the solvation entropy of Na^+ is negative, the net reaction entropy of the complete cell would also be negative. Considering that for the HC/Na metal cell studied here, the complete cell reaction entropy varies only between −10 and 6 J mol^{-1}K^{-1}, we consider a solvent cointercalation mechanism of Na^+ and diglyme in HC as unlikely. This is in accordance with dilatometry results of Escher et al., who measured rather small volume expansions of a HC composite electrode during charging [25].

A comparison of our results with the results of conventional entropy profiling studies of HC/Na metal cells by Mercer et al. [35], Wei et al. [37], and Huang et al. [38] is shown in Figure 7. The HC active materials as well as the composition of the composite electrodes used in these studies (summarized in the Supporting Information) slightly differ from each other. Additionally, in the cited studies the temperature variations took at least 10 min, which is in contrast to our stepwise temperature change of the cell within less than 1 min. Nevertheless, at SoCs above 10%, our results agree fairly well with the other studies. Similar variation of the entropy with the SoC, that is, a minimum

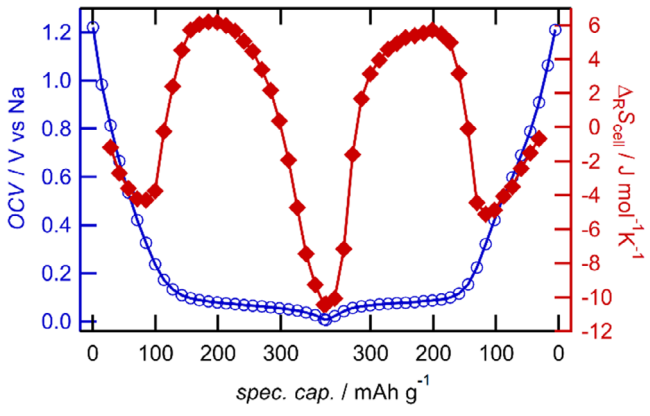

FIGURE 6 | Cell reaction entropy (filled diamonds) and OCV (circles) of a HC/Na metal coin cell with $NaPF_6$/diglyme in the charging and discharging cycle. The values at SoCs below 8% were omitted, since an accurate entropy determination was not possible, due to the sluggish kinetics of the HC composite electrode reaction.

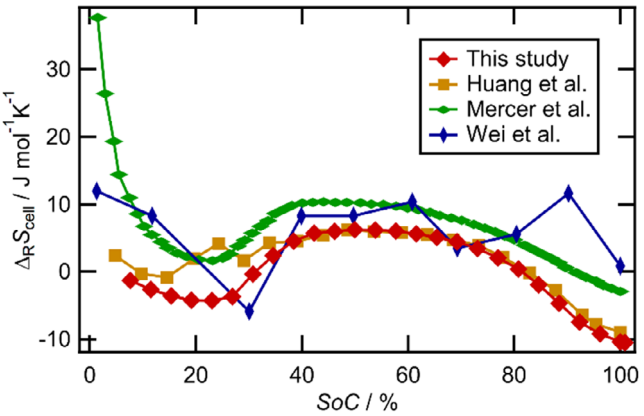

FIGURE 7 | Comparison of the cell reaction entropy obtained by different entropy profiling studies of HC/Na metal cells. Data from Huang et al. reproduced under terms of the CC-BY license from Ref [38]. Copyright 2024, IOP Publishing. Data from Mercer et al. reproduced with permission from Ref [35]. Copyright 2022, John Wiley and Sons. Data from Wei et al. reproduced with permission from Ref [37]. Copyright 2022, IOP Publishing.

at around 20% SoC followed by a broad maximum from 20% to 100%, was found by Mercer et al. [35], Huang et al. [38] and our present study. Mercer et al. explained this with a model in which simultaneous filling of the interlayer and the pores is followed by sole pore filling. This model may most likely be applicable to our study and also the one of Huang et al., although different HC materials were used in the latter investigations. However, at SoCs below 10%, significant deviations of our entropy values from the results reported by Mercer et al. can be seen. Their resting period after changing the SoC and before changing the temperature was only 20 min, so that significant base line drift of the OCV is expected. Additionally, the sluggish kinetics of the sodiation of HC at these SoCs can lead to long term variations of the OCV. Both effects render the determination of the reaction entropy difficult for SoCs < 10%.

3 | Conclusion

The cell reaction entropy of a HC composite/Na metal cell using $NaPF_6$/diglyme electrolyte solution was obtained dependent on the SoC by determining the equilibrium cell voltage shift upon fast temperature steps (rise time ca. 10 s) at open circuit conditions. The entropy ranged between −10 and +6 J $mol^{-1}K^{-1}$ which agrees with other entropy profiling studies. The rather small reaction entropy of the HC/Na metal cell indicates that during the sodiation of HC the desolvation of Na^+ is completed within 300 s independent of the SoC, that is, solvent cointercalation of diglyme in HC appears to be negligible.

In the current study we changed the temperature of the cell stepwise by switching between two temperature reservoirs. This revealed transient features in the cell voltage response, which are usually disguised in conventional entropy profiling by slow temperature changes, gradually varying on the time scale of several 10 min. In order to understand these transient features, it has to be considered that the large reaction entropies of the HC and the Na metal electrode compared to the complete cell reaction entropy lead to shifts of the single electrode potentials more than a magnitude larger than the measured cell voltage variation. Thus, differences between the temperatures of the electrodes, which occurred for $t < 60$ s after the temperature step due to the construction of the coin cell, were reflected in the cell voltage. Additionally, at low SoCs sluggish kinetics of the sodiation of HC led to a slow equilibration of the HC composite electrode potential and ultimately to a slow relaxation of the cell voltage after the temperature step. Up to now the time resolution of the experiment is limited by slow heat conduction inside the employed coin cell (thermal equilibration within 60 s). In principle, the time resolution might be improved down to a few seconds which might open perspectives for detailed kinetic studies of battery materials via the cell voltage response to temperature steps.

4 | Experimental

4.1 | Materials and Electrodes

The HC composite electrodes were prepared by spray-coating, as described in Ref [46]. A water-based slurry consisting of 85% hard carbon (Kuranode, 5 µm (type II), Kuraray, Japan) active material, 10% carbon black (Vulcan XC72R, Cabot Corporation, USA) as conductive carbon and 5% sodium carboxymethyl cellulose (CMC, molecular weight ∼124,000, Sigma–Aldrich, Germany) as binder was spray-coated onto a 50 µm Cu foil (99.995%, Advent). The electrodes were dried overnight at RT and then vacuum dried at 80°C for 12 h. The final active mass loading was 1.2–1.3 mg cm^{-2}. The counter electrode, Na metal (Alfa Aesar, Germany), was pressed on a stainless-steel spacer. The electrolyte solution was prepared by mixing 1 M $NaPF_6$ (Sigma Aldrich, Germany) in anhydrous diglyme (Sigma Aldrich, Germany).

4.2 | Coin Cells

The Stainless-steel CR2032 2-electrode coin cells were assembled in an Ar-filled glove box (MBraun, $O_2 < 0.1$ ppm and $H_2O < 0.1$ ppm). The cells consisted of a HC composite WE (diameter 12 mm), a Na metal counter electrode (diameter 12 mm), a glass fiber separator (diameter 15 mm; Whatman GF/F, United Kingdom) and 130 µl $NaPF_6$/diglyme electrolyte solution. To ensure stable cycling behavior, the cells were cycled 5 times between 0.005 and 2.0 V vs Na^+/Na with a charging rate of 0.1 C (Biologic BS-805, Biologic, France) at room temperature. All potentials are reported against Na^+/Na. The sodiation of HC is termed charging, while desodiation is termed discharging.

4.3 | Temperature Step Experiment

For the temperature step experiments, the coin cell was mounted between two aluminum blocks, which were flushed with water at a controlled temperature (see Figure S3). Two thermostats (Haake F3/K, Lauda M3), which were set to different temperatures (25.0°C and 20.7°C or 29.5°C and 20.3°C, respectively) and equipped with magnetic valves, enabled temperature changes of the aluminum blocks within less than 10 s. To follow the temperature changes, a Chromel-Alumel (Type K) thermocouple was mounted at the outside of the lower aluminum block. Together with the cell voltage, the temperature was recorded with a data logger (Agilent 34970A). A custom-built galvanostat was used to control the current to charge and discharge the cell. Experimental control and data acquisition were realized with Igor Pro.

The measurement protocol was akin to galvanostatic intermittent titration technique (GITT) with a lower voltage limit of 0.005 V and an upper voltage limit of 2.0 V. Charging/Discharging phases with a 0.05 C rate were interrupted by open circuit phases, in which the cell temperature was varied by switching between the two thermostats. In Figure S1, the voltage profile during the interrupted charging is shown. The inset of Figure S1 shows an example of a constant current charging followed by an open circuit phase together with the temperature of the cell block. The charging phase lasted 3900 s, and subsequently, the cell was set to open circuit conditions for 8100 s. During the voltage relaxation phase, the temperature was switched twice to the lower temperature for an interval of 1000 s each. For the determination of the temperature coefficient, the second temperature step was evaluated. The point of time where the temperature was switched for the second time is set to $t = 0$ s in all Figures.

Author Contributions

Laurin Derr: formal analysis (lead), investigation (supporting), methodology (lead), software (supporting), visualization (lead), writing – original

draft (lead). **Steffen Braun**: formal analysis (equal), investigation (lead), methodology (equal), writing – review and editing (supporting). **Krishnaveni Palanisamy**: resources (lead), writing – review and editing (supporting). **Christine Kranz**: funding acquisition (equal), supervision (equal), writing – review and editing (supporting). **Rolf Schuster**: conceptualization (lead), funding acquisition (lead), software (lead), supervision (lead), writing – review and editing (lead).

Acknowledgments

This work contributes to the research performed at CELEST (Center for Electrochemical Energy Storage Ulm-Karlsruhe) and was funded by the German Research Foundation (DFG) under Project ID 390874152 (POLiS Cluster of Excellence).

Open Access funding enabled and organized by Projekt DEAL.

Funding

This study was supported by Deutsche Forschungsgemeinschaft (390874152).

Conflicts of Interest

The authors declare no conflicts of interest.

Data Availability Statement

The data underlying this study are openly available in zenodo at https://doi.org/10.5281/zenodo.17591651, reference number 17591651.

References

1. A. Yao, S. M. Benson, and W. C. Chueh, "Critically Assessing Sodium-Ion Technology Roadmaps and Scenarios for Techno-Economic Competitiveness against Lithium-Ion Batteries," *Nature Energy* 10 (2025): 404–416.

2. N. Tapia-Ruiz, A. R. Armstrong, H. Alptekin, et al., "2021 Roadmap for Sodium-Ion Batteries," *Journal of Physics: Energy* 3 (2021): 031503.

3. C. Wu, Y. Yang, Y. Zhang, et al., "Hard Carbon for Sodium-Ion Batteries: Progress, Strategies and Future Perspective," *Chemical Science* 15 (2024): 6244–6268.

4. D. A. Stevens and J. R. Dahn, "High Capacity Anode Materials for Rechargeable Sodium-Ion Batteries," *Journal of the Electrochemical Society* 147 (2000): 1271.

5. C. M. Ghimbeu, A. Beda, B. Réty, et al., "Review: Insights on Hard Carbon Materials for Sodium-Ion Batteries (SIBs): Synthesis – Properties – Performance Relationships," *Advanced Energy Materials* 14 (2024): 2303833.

6. D. A. Stevens and J. R. Dahn, "The Mechanisms of Lithium and Sodium Insertion in Carbon Materials," *Journal of the Electrochemical Society* 148 (2001): A803.

7. N. Jiang, L. Chen, H. Jiang, Y. Hu, and C. Li, "Introducing the Solvent Co-Intercalation Mechanism for Hard Carbon with Ultrafast Sodium Storage," *Small* 18 (2022): 2108092.

8. Y. Aniskevich, J. H. Yu, J.-Y. Kim, S. Komaba, and S.-T. Myung, "Tracking Sodium Cluster Dynamics in Hard Carbon with a Low Specific Surface Area for Sodium-Ion Batteries," *Advanced Energy Materials* 14 (2024): 2304300.

9. Z. Lu, H. Yang, Y. Guo, et al., "Consummating Ion Desolvation in Hard Carbon Anodes for Reversible Sodium Storage," *Nature Communications* 15 (2024): 3497.

10. R. Dong, L. Zheng, Y. Bai, et al., "Elucidating the Mechanism of Fast Na Storage Kinetics in Ether Electrolytes for Hard Carbon Anodes," *Advanced Materials* 33 (2021): 2008810.

11. C. Glatthaar, M. Wang, L. Q. Wagner, et al., "Lignin-Derived Mesoporous Carbon for Sodium-Ion Batteries: Block Copolymer Soft Templating and Carbon Microstructure Analysis," *Chemistry Materials* 35 (2023): 10416–10433.

12. C. Cai, Y. Chen, P. Hu, et al., "Regulating the Interlayer Spacings of Hard Carbon Nanofibers Enables Enhanced Pore Filling Sodium Storage," *Small* 18 (2022): 2105303.

13. Y. Morikawa, S. Nishimura, R. Hashimoto, M. Ohnuma, and A. Yamada, "Mechanism of Sodium Storage in Hard Carbon: An X-Ray Scattering Analysis," *Advanced Energy Materials* 10 (2020): 1903176.

14. L. K. Iglesias, E. N. Antonio, T. D. Martinez, et al., "Revealing the Sodium Storage Mechanisms in Hard Carbon Pores," *Advanced Energy Materials* 13 (2023): 2302171.

15. Q. Gan, N. Qin, S. Gu, et al., "Extra Sodiation Sites in Hard Carbon for High Performance Sodium Ion Batteries," *Small Methods* 5 (2021): 2100580.

16. X. Chen, J. Tian, P. Li, et al., "An Overall Understanding of Sodium Storage Behaviors in Hard Carbons by an Adsorption-Intercalation/Filling Hybrid Mechanism," *Advanced Energy Materials* 12 (2022): 2200886.

17. M. A. Reddy, M. Helen, A. Groß, M. Fichtner, and H. Euchner, "Insight into Sodium Insertion and the Storage Mechanism in Hard Carbon," *ACS Energy Letters* 3 (2018): 2851–2857.

18. Z. Wang, X. Feng, Y. Bai, et al., "Probing the Energy Storage Mechanism of Quasi-Metallic Na in Hard Carbon for Sodium-Ion Batteries," *Advanced Energy Materials* 11 (2021): 2003854.

19. H. Au, H. Alptekin, A. C. S. Jensen, et al., "A Revised Mechanistic Model for Sodium Insertion in Hard Carbons," *Energy & Environmental Science* 13 (2020): 3469–3479.

20. J. M. Stratford, P. K. Allan, O. Pecher, P. A. Chater, and C. P. Grey, "Mechanistic Insights into Sodium Storage in Hard Carbon Anodes Using Local Structure Probes," *Chemical Communications* 52 (2016): 12430–12433.

21. K. Gotoh, T. Yamakami, I. Nishimura, et al., "Mechanisms for Overcharging of Carbon Electrodes in Lithium-Ion/Sodium-Ion Batteries Analysed by Operando Solid-State NMR," *Journal of Materials Chemistry A* 8 (2020): 14472–14481.

22. R. Morita, K. Gotoh, K. Kubota, et al., "Correlation of Carbonization Condition with Metallic Property of Sodium Clusters Formed in Hard Carbon Studied Using 23Na Nuclear Magnetic Resonance," *Carbon* 145 (2019): 712–715.

23. J. M. Stratford, A. K. Kleppe, D. S. Keeble, et al., "Correlating Local Structure and Sodium Storage in Hard Carbon Anodes: Insights from Pair Distribution Function Analysis and Solid-State NMR," *Journal of the American Chemical Society* 143 (2021): 14274–14286.

24. X. Yi, X. Li, J. Zhong, et al., "Unraveling the Mechanism of Different Kinetics Performance between Ether and Carbonate Ester Electrolytes in Hard Carbon Electrode," *Advanced Functional Materials* 32 (2022): 2209523.

25. I. Escher, G. A. Ferrero, M. Goktas, and P. Adelhelm, "In Situ (Operando) Electrochemical Dilatometry as a Method to Distinguish Charge Storage Mechanisms and Metal Plating Processes for Sodium and Lithium Ions in Hard Carbon Battery Electrodes," *Advanced Materials Interfaces* 9 (2022): 2100596.

26. H. Alptekin, H. Au, A. C. Jensen, et al., "Sodium Storage Mechanism Investigations through Structural Changes in Hard Carbons," *ACS Applied Energy Materials* 3 (2020): 9918–9927.

27. Z. Lv, T. Li, X. Hou, et al., "Solvation Structure and Solid Electrolyte Interface Engineering for Excellent Na+ Storage Performances of Hard Carbon with the ether-Based Electrolytes," *Chemical Engineering Journal* 430 (2022): 133143.

28. X. Li, X. Zeng, T. Ren, et al., "The Transport Properties of Sodium-Ion in the Low Potential Platform Region of Oatmeal-Derived Hard Carbon

for Sodium-Ion Batteries," *Journal of Alloys and Compounds* 787 (2019): 229–238.

29. K. Schutjajew, T. Tichter, J. Schneider, M. Antonietti, C. Roth, and M. Oschatz, "Insights into the Sodiation Mechanism of Hard Carbon-Like Materials from Electrochemical Impedance Spectroscopy," *Physical Chemistry Chemical Physics* 23 (2021): 11488–11500.

30. R. Väli, A. Jänes, and E. Lust, "Alkali-Metal Insertion Processes on Nanospheric Hard Carbon Electrodes: An Electrochemical Impedance Spectroscopy Study," *Journal of the Electrochemical Society* 164 (2017): E3429.

31. F. Linsenmann, D. Pritzl, and H. A. Gasteiger, "Comparing the Lithiation and Sodiation of a Hard Carbon Anode Using In Situ Impedance Spectroscopy," *Journal of the Electrochemical Society* 168 (2021): 010506.

32. L. Derr, M. Lang, K. Palanisamy, C. Kranz, and R. Schuster, "Role of Desolvation upon the Sodiation of Hard Carbon in Sodium-Ion Batteries: A Microcalorimetric Study of the Sodiation Entropy," *The Journal of Physical Chemistry C* 129 (2025): 4025–4031.

33. J. R. Dahn and R. R. Haering, "Entropy Measurements on Li_xTiS_2," *Canadian Journal of Physics* 61 (1983): 1093–1098.

34. A. J. Bard and L. R. Faulkner, *Electrochemical Methods: Fundamentals and Applications*, (Wiley, 2001).

35. M. P. Mercer, S. Affleck, E. M. Gavilán-Arriazu, et al., "Sodiation Of Hard Carbon: How Separating Enthalpy and Entropy Contributions Can Find Transitions Hidden In the Voltage Profile," *ChemPhysChem* 23 (2022): 202100748.

36. M. P. Mercer, M. Nagarathinam, E. M. Gavilán-Arriazu, et al., "Sodiation Energetics in Pore Size Controlled Hard Carbons Determined via Entropy Profiling," *Journal of Materials Chemistry A* 11 (2023): 6543–6555.

37. F. Wei, P. Li, Q. Zhang, G. Shao, and J. Mao, "Entropy Change Characteristics for Sodium Ion Half/Full Cells Based on Na3V2(PO4)3 and Hard Carbon Materials," *Journal of the Electrochemical Society* 169 (2022): 050503.

38. J. Huang, C. Delacourt, P. Desai, and J.-M. Tarascon, "Operando Entropy Profiling of Sodium-Ion Batteries via Optical Fiber Sensing for Thermal Management and Ageing Monitoring," *Journal of the Electrochemical Society* 171 (2024): 030516.

39. R. Mogensen, D. Brandell, and R. Younesi, "Solubility of the Solid Electrolyte Interphase (SEI) in Sodium Ion Batteries," *ACS Energy Letters* 1 (2016): 1173–1178.

40. L. A. Ma, A. J. Naylor, L. Nyholm, and R. Younesi, "Strategies for Mitigating Dissolution of Solid Electrolyte Interphases in Sodium-Ion Batteries," *Angewandte Chemie International Edition* 60 (2021): 4855–4863.

41. P. J. Osswald, M. del Rosario, J. Garche, A. Jossen, and H. E. Hoster, "Fast and Accurate Measurement of Entropy Profiles of Commercial Lithium-Ion Cells," *Electrochimica Acta* 177 (2015): 270–276.

42. F. Karcher, M. Uhl, T. Geng, T. Jacob, and R. Schuster, "Entropic Contributions to Sodium Solvation and Solvent Stabilization upon Electrochemical Sodium Deposition from Diglyme and Propylene Carbonate Electrolytes," *Angewandte Chemie International Edition* 135 (2023): 202301253.

43. J. N. Agar, in *Advances in Electrochemistry and Electrochemical Engineering*, ed. P. Delahay, (Interscience Publishers, 1963), pp. 31–121.

44. W. Schmickler and E. Santos, *Interfacial Electrochemistry*, (Springer, 2010).

45. Y. Niu, J. Yang, F. Meng, et al., "Deciphering and Enhancing Rate-Determining Step of Sodium Deposition towards Ultralow-Temperature Sodium Metal Batteries," *Angewandte Chemie International Edition* 64 (2025): e202416720.

46. K. Palanisamy, S. Daboss, D. Schäfer, et al., "Spray-Coated Hard Carbon Composite Anodes for Sodium-Ion Insertion," *Batteries & Supercaps* 7 (2024): e202300402.

Supporting Information

Additional supporting information can be found online in the Supporting Information section. **Supporting Fig. S1**: Cell voltage during the GITT-type charging with constant current (CC) phases (charging rate 0.05 C) followed by open circuit (OC) phases. The inset shows a charging and an open circuit phase together with the temperature of the aluminum cell holder in detail. **Supporting Fig. S2**: Cell voltage transients at open circuit conditions due to a temperature step from 25.0°C to 20.7°C (dark blue) and from 29.5°C to 20.3°C (light blue) of a fully sodiated HC/Na metal cell (SoC 99%). **Supporting Fig. S3**: Schematic of the experimental setup used for the temperature step experiments. A coin cell was clamped between two aluminum blocks (1 and 8), which were flushed with water either from a warm or a cool reservoir. The stainless-steel coin cell consisted of a top cap (2), a HC composite electrode on a Cu current collector (3), a glass fiber separator soaked with the electrolyte solution (4), a stainless-steel spacer with the Na metal on top (5), a stainless-steel spring (6) and a bottom cap (7). **Supporting Fig. S4**: Detail of the cell voltage transient at open circuit conditions during the charging cycle at a SoC of 19%. The blue dashed line indicates the drift at the lower temperature (20.7°C, linear fit from $t = 300$ s to $t = 1000$ s). The black arrow shows the cell voltage difference ΔE_0 at $t = 0$ s used for the determination of $\Delta_R S_{cell}$. **Supporting Fig. S5**: Cell reaction entropy of a HC/Na metal cell with $NaPF_6$/diglyme dependent on the OCV in the charging and the discharging cycle. **Supporting Fig. S6**: Comparison of the cell reaction entropy (filled diamonds) and the OCV (circles) during the charging cycle of two different HC/Na metal cells with $NaPF_6$/diglyme (S1 and S3), and of the same cell but different temperature step heights used for the temperature steps. **Supporting Fig. S7**: Electric equivalent circuit used for the coin cell temperature simulation. **Supporting Table S1**: Parameters used for the coin cell temperature simulation. **Supporting Table S2**: Parameters used in the simulation of the single electrode potentials.